Published in final edited form as:
Neuroscience. 2011 January 13; 172: 427–442. doi:10.1016/j.neuroscience.2010.10.035.

Pik3c3 deletion in pyramidal neurons results in loss of synapses, extensive gliosis and progressive neurodegeneration

Liangli Wang[1], **Katie Budolfson**[1], and **Fan Wang**[1,*]

[1] Department of Cell Biology, Duke University Medical Center, Box 3709, Durham, NC 27710

Abstract

The lipid kinase PIK3C3 (also known as VPS34) regulates multiple aspects of endo-membrane trafficking processes. PIK3C3 is widely expressed by neurons in the central nervous system (CNS), and its catalytic product PI3P is enriched in dendritic spines. Here we generated a line of conditional mutant mouse in which *Pik3c3* is specifically deleted in hippocampal and in small subsets of cortical pyramidal neurons using the *CaMKII-Cre* transgene. We found that *Pik3c3*-deficiency initially causes loss of dendritic spines accompanied with reactive gliosis, which is followed by progressive neuronal degeneration over a period of several months. Layers III and IV cortical neurons are more susceptible to *Pik3c3*-deletion than hippocampal neurons. Furthermore, in aged conditional *Pik3c3* mutant animals, there are extensive gliosis and severe secondary loss of wildtype neurons. Our analyses show that *Pik3c3* is essential for CNS neuronal homeostasis and *Pik3c3*$^{flox/flox}$;*CaMKII*-Cre mouse is a useful model for studying pathological changes in progressive forebrain neurodegeneration.

Keywords

PIK3C3/Vps34; synapse; pyramidal neuron; neurodegeneration; reactive gliosis

INTRODUCTION

Neurons contain extensive amount of surface membranes due to their elaborate dendritic and axonal arbors. Endocytic membrane trafficking plays essential roles not only in maintaining neuronal morphological integrity, but also in cycling molecular components involved in neurotransmission and in trafficking receptors at the postsynaptic sites (De Camilli and Takei, 1996; Barry and Ziff, 2002; Malinow and Malenka, 2002; Bredt and Nicoll, 2003). Alterations in endosomal functions have been observed in a range of neurodegenerative disorders (Soreghan et al., 2003; Nixon, 2005; Bronfman et al., 2007; Lee et al., 2007).

The class III phosphoinositide 3-kinase (PIK3C3, also known as VPS34) is a member of the PI3K family lipid kinases. It specifically utilizes phosphatidylinositol as a substrate, producing the single lipid product phosphatidylinositol-3-phosphate (PI3P) (Wurmser et al., 1999). PI3P is highly enriched on early endosomes and multivesicular bodies (MVBs) and can recruit proteins containing FYVE, PX or PH motifs to these compartments (Gaullier et al., 1998; Patki et al., 1998; Gillooly et al., 2000). In invertebrate organisms and non-

*Correspondence should be addressed to: Fan Wang (f.wang@cellbio.duke.edu).

neuronal cells, PI3P and PIK3C3 were shown be involved in endocytic vesicular trafficking and intracellular protein sorting (Herman and Emr, 1990; Takegawa et al., 1995; Gruenberg and Stenmark, 2004; Johnson et al., 2006; Juhasz et al., 2008), as well as in the initiation of autophagy (Petiot et al., 2000; Levine and Klionsky, 2004; Zeng et al., 2006). In addition, PIK3C3 is also required for nutrient activation of mTOR signaling in cultured cells (Nobukuni et al., 2007; Gulati et al., 2008). Recently, a genetic study of *Pik3c3* in mammals showed that deletion of *Pik3c3* in differentiated sensory neurons causes neuronal subtype specific degenerative phenotypes, mainly due to a disruption in the endosomal but not the autophagy pathway, indicating that PIK3C3-regulated endosomal pathway is essential for sensory neuron survival and homeostasis (Zhou et al., 2010). The consequences of *Pik3c3* deletion in CNS neurons have not been characterized.

The *Pik3c3* gene is widely expressed in the developing (Zhou et al., 2010) and adult brain (http://mouse.brain-map.org/brain/Pik3c3/68498253/thumbnails.html). Moreover, PI3P is ubiquitously distributed in both dendrites and axons in cultured hippocampal neurons, with an enrichment in spines as shown by its co-localization with the postsynaptic marker PSD95 (Figure 1A and 1B). To examine the roles of PIK3C3 in the maintenance of synaptic and neuronal homeostasis, we specifically deleted *Pik3c3* in mature pyramidal neurons by crossing the *CaMKII-Cre* transgenic mice with the *Pik3c3*$^{flox/flox}$ conditional null mice. Here we report our analyses of the *CaMKII-Cre; Pik3c3*$^{flox/flox}$ conditional mutant mice and show that these mice are useful models to study progressive forebrain neurodegeneration.

EXPERIMENTAL PROCEDURES

Mouse strains

Pik3c3$^{flox/flox}$ mice (described previously Zhou et al., 2010) were crossed with *CaMKII-Cre* transgenic mice (Xu et al., 2000). At 4 weeks of age, tail tissue was taken from the mice for genotyping. In all experiments, conditional mutants (*CaMKII-Cre; Pik3c3*$^{flox/flox}$) were compared to heterozygous *CaMKII-Cre; Pik3c3*$^{flox/+}$ littermates. At each stage/age, 6 pairs (conditional mutants and heterozygous controls) of mice were used for H&E, immunostaining and Golgi staining, respectively. To analyze the pattern of Cre-mediated recombination, *CaMKII-Cre* mice were crossed to the *Rosa*$^{CAG\text{-}STOP\text{-}tdTomato}$ reporter mice (hereafter shortened as *Rosa*$^{stop\text{-}tdTomato}$ mice). All experimental procedures were approved by the Institutional Animal Care and Use Committee of Duke University.

Neuron culture

Dissociated hippocampal cultures were prepared from 1-d-old mice as described previously (Oh and Derkach, 2005) and transfected after 13 days in vitro (DIV) using a lipofectamine 2000 transfection protocol. Briefly, for a 12-well plate, 160 μl of Neurobasal per well was combined with 3.2 ul of LIPOFECTAMINE 2000 and allowed to sit at room temperature for 5 min. Then, the solution was combined with 1 μg DNA in 160 μl of Neurobasal and allowed to sit at room temperature for 20 min (all transfection materials from Invitrogen, Rockville, MD). While the solutions were complexing, the cultures were removed from the incubator and the medium was replaced with 2 ml Neurobasal. Twenty minutes later, the DNA/lipofectamine mixture was added to the culture. After 30–45 min incubation, the medium was replaced with normal culture medium. The generation of plasmid constructs expressing mVenus-2xFYVE or mCherry has been described (Zhou et al., 2010).

Tissue processing

Mice were overdosed with anesthetic and intracardially perfused with cold saline, followed by 4% paraformaldehyde. Brains were removed, post-fixed overnight. For H&E staining, fixed brain tissues were dehydrated in ethanol, embedded in paraffin. For

immunocytochemistry, fixed brains were then stored in 30% sucrose at 4°C. For Golgi staining, mice were only slightly perfused. Brains were removed and placed in Golgi solution (FD NeuroTechnologies).

Histological Methods

For H&E staining, fixed brain tissues were serially sectioned at 7 μm, and stained with hematoxylin (Sigma) and eosin (Sigma). For immunocytochemistry, brains were cut into 20 μm coronal sections on a Cryostat. Every 6^{th} coronal sections were collected encompassing frontal to visual cortex and the corresponding subcortical regions. For each sample, six to eight analogous sections were randomly chosen for staining and analyses. Standard immunofluorescence procedure is used. Antibodies used include anti-PSD95 (Chemicon, 1:500), monoclonal anti-NeuN antibody (Chemicon, 1:1000), rabbit anti-caspase 3 active (R&D Systems, 1:500), rabbit anti-parvalbumin (Swant, 1:5000), rabbit anti-GFAP (DAKO, 1:500), Alexa Fluor 488-conjugated goat anti-rabbit IgG (Invitrogen, 1:400) and Alexa Fluor 568-conjugated goat anti-mouse IgG (Invitrogen, 1:400).

In situ hybridization

The cDNA fragments used for in situ hybridization against Etv1, Wfs1, Cart, Rorb and TC1460681gene, were individually cloned by PCR. Antisense riboprobes labeled with digoxygenin (DIG)-UTP or fluorescein (FITC)-UTP (Roche) were transcribed as described previously (Zhou et al., 2010). In situ hybridization using DIG labeled probes and fluorescent in situ hybridization using FITC labeled probes were performed according to standard methods.

Electron microscopy

Mice were killed and perfused with PBS followed by 2% paraformaldehyde and 2.5% glutaraldehyde in 0.1M phosphate buffer. Brains were removed and postfixed in the buffer for 3 days. Following dissection and fixation for 2 hr in 1% osmium tetroxide (Electron Microscopy Sciences) plus 1.5% potassiumferrocyanide (Electron Microscopy Sciences), the tissues were dehydrated using a series of ethanol dilutions and embedded in an Epon-propyleneoxide mixture. Ultrathin sections were cut using a Reichert Ultracut S microtome, and sections were examined at a Philips CM 12 electron microscope. The CA1 pyramidal cell layer of the hippocampus was identified first at low magnification and EM images were collected from the apical dendrite layer (at a distance of 100–200 μm from the pyramidal cell bodies). For quantitative analysis, randomly positioned 40 images per section in defined region of hippocampus were collected (with the genotype blind to the person taking images). The number and length of postsynaptic densities (only thickened densities of asymmetric synapses were counted) and width of the synaptic cleft were measured while the genotypes were blind to the experimenter using Metamorph software.

Quantitative analyses

To quantify the relative density of neurons expressing a layer-specific marker, positive cells within 0.5mm width column spanning all layers of the cortex on 20 μm sections were counted and data were expressed as cell numbers per $0.01mm^2$.

To determine spine density, dissected brains were placed in Golgi solution for 12 days (FD NeuroTechnologies). Vibratome sections (100 μm) were collected from the hippocampal region and randomly selected images of dendrites within the area of CA1 stratum radiatum were taken using a 63× objective with a Leica microscope. Using Metamorph software, a dendritic region that was clearly in focus was traced to measure its length. The number of spines on that region was counted and divided by the length to obtain spine density.

Data are presented as means ± SD or SEM. Statistical significance was assessed by two-tailed Student's *t*-test. The level of significance was set at $P < 0.05$.

RESULTS

PI3P is present in both dendrites and axons and partially co-localizes with PSD95 in cultured hippocampal neurons

Pik3c3 is widely expressed in developing (Zhou et al., 2010) and adult brain. To visualize the cellular distribution of its product PI3P in pyramidal neuron, we co-transfected hippocampal neurons with a construct containing a Venus (green) tagged tandem FYVE domains that binds PI3P with high specificity (Petiot et al., 2003) and mCherry (red) at 13 days in vitro (DIV). As shown in Figure 1A, Venus-2xFYVE signals were abundantly detected in the soma and dendrites (the picture was highly over-exposed intentionally to reveal the PI3P distribution in high order branches) with punctae-like fluorescence signals observed in higher order branches (Figure 1A). In the axon, very faint dotted-like fluorescence signals were detected (insert in Figure 1A). Immunostaining using antibody against postsynaptic marker PSD95 revealed that PI3P is enriched at the postsynaptic sites (Figure 1B). Venus-2xFYVE is not detectable in distal axon termini when moderately expressed, whereas high-level expression of venus-2xFYVE was toxic to the cultured neurons. Thus, we could not examine whether PI3P is present at the pre-synaptic sites. The pattern of PI3P distribution in neurons suggests that PIK3C3 actively produce PI3P in both dendrites and axons, and perhaps is particular active at synapses (dendritic spines).

Generating mice with forebrain-specific disruption of the *Pik3c3* gene in subpopulations of pyramidal neurons

To examine the possible role of PIK3C3/PI3P in maintaining synaptic and neuronal homeostasis, we crossed $Pik3c3^{flox/flox}$ conditional mice (Zhou et al., 2010) with the *CaMKII-Cre* transgenic mice in which the Cre recombinase is expressed under the control of calcium-dependent calmodulin kinase II promoter (Xu et al., 2000). To visualize the Cre expression pattern, we crossed *CaMKII-Cre* line with the $Rosa^{stop\text{-}tdTomato}$ reporter mice. Expression of the tomato reporter was detected as early as postnatal 14 days (P14). At this age, very few cells expressing tomato were seen in the cortex and in the hippocampus (Figure 2A, left panels). At P28, the number of tomato-expressing cells reached a plateau in both cortex and hippocampus (Figure 2A, right panels). After P28, we did not observe any further increase in Cre expressing neurons (data not shown). At P28 and later stages, about 22.8% of neurons (percentage of tomato-expressing in NeuN-positive cells) in the cortex, mainly in layer II/III, IV and VI, display Cre-mediated tomato expression. We noticed that layer V in cortex contained a very sparse number of reporter expressing cells (arrow in Figure 2A). To further confirm this observation, we performed two-color in situ hybridization with probes for the layer V marker Etv1 and tomato. Indeed, Etv1 marked the layer where the least number of tomato expressing cells were observed (Arrow in Figure 2B). Thus, Etv1-positive layer V cortical neurons should be the least affected in the *CaMKII-Cre;* $Pik3c3^{flox/flox}$ conditional mutant mice. In hippocampus, the majority of CA1 pyramidal neurons (more than 95%) expressed tomato, whereas only a very small number of neurons in CA3 and dentate gyrus had Cre activity (Figure 2A). The expression pattern of tomato reporter is largely consistent with previously described for this Cre line (Xu et al., 2000).

Consistent with the temporal expression pattern of Cre in the hippocampus, the mRNA level of *Pik3c3* in CA1 region at P14 in *CaMKII-Cre;* $Pik3c3^{flox/flox}$ mice (hereafter designated as *Pik3c3*-cKO) was comparable to that in the littermate heterozygous *CaMKII-Cre;* $Pik3c3^{flox/+}$ mice (controls) (data not shown), but was largely diminished at P28 (Figure

2C). The *Pik3c3*-cKO mice are viable, fertile, and survived at least to 9 months of age. They show no gross abnormalities in size or weight compared to the controls.

The development of dendritic morphology and dendritic spines of CA1 hippocampal neurons is normal in *Pik3c3*-cKO mutant

Using various histological examinations including H&E staining, in situ hybridization with layer specific markers, anti-NeuN staining (neuron specific marker), anti-GFAP staining (glial markers), and Golgi staining, we did not observe any molecular or morphological differences between control and *Pik3c3-cKO* cortex and hippocampus up to 6-weeks of age (Figure 3A–C, and data not shown). Even the spine density of hippocampal CA1 neurons as assessed by Golgi staining is unchanged in the mutant at this young age. On average, there were 1.51 ± 0.15 spines/μm in controls and 1.48 ± 0.12 spines/μm in *Pik3c3*-cKO ($P = 0.49$) at 6-week of age (Figure 3C right). To determine whether there might be ultra-structural changes at the synapse level that were not detectable by light microscopy, we performed electron microscopy analysis of the CA1 apical dendrite region from 6 week-old mice. We found that the number or the length of postsynaptic densities, or the width of the synaptic cleft in CA1 neurons is comparable between control and *Pik3c3-cKO* mice at this age (Figure 3D). Taken together, neuronal morphogenesis and spine formation is not affected by *CaMKII-Cre* mediated deletion of *Pik3c3*.

Loss of dendritic spines and reactive gliosis occurred before significant loss of neurons in hippocampus in 11-week old mutant

Interestingly, at 11-weeks of age (7 weeks after *Pik3c3* deletion in more than 95% of CA1 neurons), we did not detect any statistically significant loss of neurons in the CA1 region of hippocampus (Figure 4A). This is in contrast to the rapid neurodegeneration of *Pik3c3*-deficient sensory neurons (die within 2 weeks after *Pik3c3*-deletion) that we reported previously (Zhou et al., 2010). However, anti-GFAP staining revealed significantly elevated GFAP signal across the hippocampus, suggesting a marked increase in reactive gliosis (Figure 4A). Since glial cells do not express *CaMKII-Cre* and hence they are wildtype, this reactive gliosis must be a response to some pathological changes of hippocampal neurons (prior to the loss of neurons). We therefore examined the fine scale morphology of CA1 neurons. As revealed by Golgi staining, the gross dendritic morphology in *Pik3c3*-cKO appeared normal when compared with pyramidal neurons located at similar location in control mice (Figure 4B). However, there are fewer and shorter spines on the apical dendrite of CA1 neurons in the mutant at this age (Figure 4C). We counted the spines from the first order branches within lucidum-radiatum region of CA1 and found on average, a 20% reduction in spine density in the mutant (1.53 ± 0.17 in control versus 1.25 ± 0.24 spines/um in mutant, $P<0.001$) (Figure 4C right). Thus, the loss of spines/synapses and reactive gliosis precede the significant loss of hippocampal neurons in the *Pik3c3-cKO* mutant. This phenotype resembles that observed in many neurodegenerative disorders such as the Alzheimer's disease (Games et al., 1995).

Substantial hippocampal neuronal loss and extensive gliosis in 6–9 month old *Pik3c3*-cKO mice

At the age of 6 months, both H&E staining and anti-NeuN staining revealed that the pyramidal neuron layer in CA1 region of the hippocampus in *Pik3c3*-cKO mice was significantly thinner (Figure 5A–B, arrowheads delineate the boundaries of CA1), and quantification showed a substantial loss of neurons (Figure 5C), whereas other regions of hippocampus appeared normal and intact at this stage (Figure 5A–B). This is consistent with the fact that *CaMKII-Cre* is primarily expressed in the CA1 region. Furthermore, anti-GFAP staining revealed extensive gliosis across the entire hippocampus (albeit to a lesser extent in the CA2 region) (Figure 5B). These results indicate that PIK3C3 is required for maintaining

neuronal homeostasis in mature neurons and *Pik3c3* deficiency causes progressive degeneration of hippocampal pyramidal neurons. Similar pathological changes were observed in 9-month old mutant mice. In addition, substantial neuronal loss was observed in all regions of hippocampus including in CA3 and dentate gyrus at this stage (data not shown).

Loss of layer III-IV cortical neurons and reactive gliosis in 11-week old *Pik3c3*-cKO mice

In contrast to the somewhat resilience of CA1 hippocampal neurons upon *Pik3c3* deletion, apparent pathological changes were observed in the cerebral cortex of mutant mice as early as 11-week old. As shown in Figure 6A, the thickness of the cortex in *Pik3c3*-cKO mouse is about 80% of that in control mouse at this stage. A large number of pyknotic or darkly stained nuclei (by H&E method) were detected in the mutant cortex. Immunostaining using anti-GFAP antibody showed very weak signal in control cortex. By contrast, astrocytes express high level GFAP in the mutant. The reactive astrocytes are mostly present in layers III, IV, VI and to a less extent in layer II and V (Figure 6B). To better visualizing the cortical layers, we performed in situ hybridization with layer specific probes: layer II-Wfs1 (Wolfram syndrome 1 homolog), layer IIIb-Cart (cocaine and amphetamine regulated transcript), layer IV-Rorb (RAR-related orphan receptor beta), layer V-Etv1, and layer VI-TC1460681 (Lein et al., 2007). We found that there was a 50% reduction in the number of neurons expressing layer IIIb marker Cart, and a 10% reduction in cells expressing layer IV marker Rorb (Figure 7A–B). Other layers are not significantly affected suggesting layer III and IV cortical neurons are most vulnerable to *Pik3c3*-deletion.

Extensive cortical neuronal loss and reactive gliosis in 6-month old *Pik3c3*-cKO mice

Somewhat unexpectedly, even though *Pik3c3* is only deleted in less than 23% of neurons in the cortex using this *CaMKII-Cre* line, the cortex from 6-month old mutant was significantly thinner (about 60% of the thickness of control cortex) as revealed by both H&E and anti-NeuN staining. There is an overall more than 40% reduction in the number of cortical neurons, suggesting that both *Pik3c3*-deficient as well as wildtype neurons are lost. Numerous cells showed darkly stained nuclei in the mutant mice (Figure 8A left panel). In situ hybridization with layer specific markers revealed the loss of 50% neurons from both layer III and IV, as well as a 40% reduction of layer VI neurons (Figure 8C). The numbers of cells expressing layer II and layer V markers were comparable between control and mutant mice (Figure 8C). Because *CaMKII-Cre* mediated gene deletion occurs specifically in pyramidal neurons (Xu et al., 2000), as a control, we examined the number of cells expressing parvalbumin, an interneuron marker (Hendry et al., 1989). Notably, the density of parvalbumin expressing cells appeared increased in mutant because the cortex was compressed due to the loss of pyramidal neurons (Figure 8C). When factor in the reduced total volume of brain, the number of parvalbumin-positive cells was about the same as that in controls at this stage. Since *CaMKII-Cre* only expresses in very few scattered cells in layer V, it is not unexpected that layer V cells were largely intact. This could also explain the fact that 6-month old mutant mice did not show any obvious movement defects. Finally, anti-GFAP staining showed continued extensive gliosis in the cortex at this age (Figure 8B).

Moreover, when we examined apoptosis using immunostaining against anti-active caspase 3, we rarely observed active apoptotic cells in *Pik3c3-cKO* cortex at both 6- and 9-month of age (data not shown). Thus the degenerating neurons do not appear to undergo massive apoptosis, and we suspect that they might be actively taken away by macrophages/microglial cells.

Further wide-spread secondary loss of all types of neurons in 9-months old Pik3c3-cKO mice

Results from 6 months old mutant mice suggested that there is significant secondary loss of wildtype neurons in the aged mutant mice. This could be due to several possible reasons: (1) wildtype neurons that are synaptic partners of the mutant neurons degenerate after the death of the mutant neurons due to the loss of synaptic target-derived trophic support; (2) dying mutant neurons release cytotoxic factors that lead to the secondary degeneration of wildtype neurons; and (3) the reactive astrocytes initially triggered by the mutant neurons release cytotoxic molecules such as reactive oxygen species, which in turn caused damage and death of otherwise healthy neurons (Viviani et al., 2001; Chvatal et al., 2008; Sofroniew, 2009). Regardless of which mechanism is primarily responsible for the secondary loss of wildtype neurons, it appears to be a vicious cycle, as secondary death of neurons will trigger further degeneration of neurons. Therefore, we predicted that the effects of this vicious cycle would spread further to cause the death of all types of neurons.

Indeed, in 9-month old mutant, neurons from all cortical layers show severe reduction in numbers (Figure 9–10), even parvalbumin-expressing interneurons are significantly lost compared to 6-month old animals (Figure 10, factor in significant reduction of the total cortical volume). Overall, about 30% neurons are left in the cortex, and extensive gliosis covers the cortex.

Discussion

In this study, we specifically deleted the *Pik3c3/Vps34* gene in 95% neurons in the CA1 region of hippocampus and in 23% of postnatal pyramidal neurons in the cortex using the Cre/LoxP strategy. After reaching maximal *CaMKII-Cre* mediated *Pik3c3* deletion, which occurs around 4 weeks postnatally, mutant neurons gradually lost spines between 6 to 11 weeks, neurons degenerate progressively, and reactive gliosis is triggered. The loss of spines is likely a result of disrupted endocytic trafficking at both pre- and post-synaptic sites. Furthermore, the *Pik3c3*-deleted neurons degenerate first, which induces further extensive gliosis and secondary loss of otherwise normal neurons, and eventually leads to massive atrophy of the entire cortex and hippocampus (summarized in Figure 11).

The phenotypes observed in the *CaMKII-Cre* mediated *Pik3c3* deletion mouse are quite different from what we have seen in the *Pik3c3*-deficient sensory neurons where abnormally enlarged vesicles or vacuoles accumulate in a subset of sensory neurons and trigger rapid degeneration of these neurons within 2-weeks of age (Zhou et al., 2010). In the mouse model presented in this study, *Pik3c3*-deficient CA1 hippocampal neurons slowly lose dendritic spines and undergo a progressive degeneration over a period of many weeks to several months. These differences may result from the different timing of Cre-mediated deletion. In the case of sensory neurons, *Pik3c3* is deleted at birth, when the sensory neurons are still extending axons as the animals undergo rapid postnatal growth in body size. In this study, *CaMKII-Cre* mediated deletion happens between 3~4 weeks of age in mature neurons, and thus PIK3C3-mediated endocytic trafficking may play a more restricted and specialized functions at the pre- and post-synaptic termini. We also observed that certain layers of cortical neurons appear more susceptible than CA1 hippocampal neurons, as the loss of neurons in layers III and IV were observed a few weeks after *Pik3c3*-deletion. The cell type dependent differences in susceptibility to a genetic mutation are not rare. In fact, in all degenerative and aging processes, there are always some populations of neurons more vulnerable than others although the mutated gene is expressed ubiquitously (Skibinski et al., 2005; Chandran et al., 2007; Spinosa et al., 2008). However, the cellular and molecular basis for such differential vulnerability of neurons in response to generic mutation is not clear.

Neurons often need to receive trophic support from their axonal targets and endosomes are increasingly recognized as important carriers for such growth/survival factor signaling (Cosker et al., 2008; Wu et al., 2009). PIK3C3-deficiency thus could affect the formation signaling endosomes and prevents the trophic signaling from reaching the cell body. This may be one possible explanation for the progressive neurodegeneration phenotypes observed in this study. Furthermore, in addition to its role in endocytic and autophagic pathways, PIK3C3/Vps34 was shown to mediate nutrient signaling to mTOR (mammalian targets of rapamycin) (Nobukuni et al., 2007). Briefly, nutrients, such as amino acids and glucose, induce a rise in intracellular calcium that activates the lipid kinase activity of PIK3C3. PIK3C3 and its product PI3P are required to activate mTOR and its downstream effector S6 kinase 1, which results in elevated levels of protein synthesis and increased cell growth (Gulati et al., 2008). Since mTOR plays important roles in regulating dendritic protein synthesis, synapse formation, synaptic plasticity, and learning and memory (Cammalleri et al., 2003; Kelleher et al., 2004; Takei et al., 2004; Gong et al., 2006; Parsons et al., 2006; Slipczuk et al., 2009), the observed loss of dendritic spines could partly result from a secondary defect caused by the lack of mTOR signaling in mutant neurons.

Neurodegenerative diseases are characterized by loss of selective neuronal populations and reactive gliosis. Several animal models have been generated to mimic the pathological development of neurodegenerative diseases, including Huntington's disease (Reddy et al., 1998) and Alzheimer's disease (Games et al., 1995). Interestingly, our mouse model shares some striking similarities with those models as well with many neurodegenerative diseases, in which affected neurons lose synapses and die progressively and extensive reactive gliosis occurs. Moreover, we show that although only 23% of cortical pyramidal neurons are mutated by *CaMKII-Cre* mediated deletion of *Pik3c3* which results in the initial loss of these mutant neurons, there is a significant secondary death of wildtype pyramidal and interneurons such that by 9-month of age, only 30% neurons are left in the cortex. The exact mechanisms underlying the secondary loss of neurons are not clear and are likely to involve the reactive gliosis (Pekny and Nilsson, 2005; Chvatal et al., 2008; Sofroniew, 2009). Nonetheless, this result has important implications for understanding the etiology and progression of age-dependent neurodegenerative diseases. It suggests that an initial loss of small population of neurons can trigger reiterative cycles of secondary loss of otherwise normal neurons. Thus, preventing the secondary loss of neurons may be a key to slow or stop the progression of neurodegeneration diseases such as the Alzheimer's diseases. In the future, it would be interesting to test whether inhibiting reactive gliosis in our mouse model could prevent the secondary loss of neurons.

Acknowledgments

We thank the Duke Pathology EM facility for help with EM analysis. We also thank Xiang Zhou, Alexandra Scott, Susana da Silva and Bao-Xia Han for many technical helps as well as valuable suggestions and comments on the manuscript. This work is supported by the McKnight Scholar Award, the Wings for Life Foundation, and an RO1 from NIDCR all to F.W.

Abbreviations

PIK3C3	class III phosphoinositide 3-kinase
PtdIns3P	phosphatidylinositol-3-phosphate
DIV	days in vitro
Wfs1	Wolfram syndrome 1 homolog
Cart	cocaine and amphetamine regulated transcript

Rorb	RAR-related orphan receptor beta
Etv1	ets variant gene 1

References

Barry MF, Ziff EB. Receptor trafficking and the plasticity of excitatory synapses. Curr Opin Neurobiol. 2002; 12:279–286. [PubMed: 12049934]

Bredt DS, Nicoll RA. AMPA receptor trafficking at excitatory synapses. Neuron. 2003; 40:361–379. [PubMed: 14556714]

Bronfman FC, Escudero CA, Weis J, Kruttgen A. Endosomal transport of neurotrophins: roles in signaling and neurodegenerative diseases. Dev Neurobiol. 2007; 67:1183–1203. [PubMed: 17514710]

Cammalleri M, Lutjens R, Berton F, King AR, Simpson C, Francesconi W, Sanna PP. Time-restricted role for dendritic activation of the mTOR-p70S6K pathway in the induction of late-phase long-term potentiation in the CA1. Proc Natl Acad Sci U S A. 2003; 100:14368–14373. [PubMed: 14623952]

Chandran J, Ding J, Cai H. Alsin and the molecular pathways of amyotrophic lateral sclerosis. Mol Neurobiol. 2007; 36:224–231. [PubMed: 17955197]

Chvatal A, Anderova M, Neprasova H, Prajerova I, Benesova J, Butenko O, Verkhratsky A. Pathological potential of astroglia. Physiol Res. 2008; 57(Suppl 3):S101–110. [PubMed: 18481910]

Cosker KE, Courchesne SL, Segal RA. Action in the axon: generation and transport of signaling endosomes. Curr Opin Neurobiol. 2008; 18:270–275. [PubMed: 18778772]

De Camilli P, Takei K. Molecular mechanisms in synaptic vesicle endocytosis and recycling. Neuron. 1996; 16:481–486. [PubMed: 8785046]

Games D, Adams D, Alessandrini R, Barbour R, Berthelette P, Blackwell C, Carr T, Clemens J, Donaldson T, Gillespie F, et al. Alzheimer-type neuropathology in transgenic mice overexpressing V717F beta-amyloid precursor protein. Nature. 1995; 373:523–527. [PubMed: 7845465]

Gaullier JM, Simonsen A, D'Arrigo A, Bremnes B, Stenmark H, Aasland R. FYVE fingers bind PtdIns(3)P. Nature. 1998; 394:432–433. [PubMed: 9697764]

Gillooly DJ, Morrow IC, Lindsay M, Gould R, Bryant NJ, Gaullier JM, Parton RG, Stenmark H. Localization of phosphatidylinositol 3-phosphate in yeast and mammalian cells. EMBO J. 2000; 19:4577–4588. [PubMed: 10970851]

Gong R, Park CS, Abbassi NR, Tang SJ. Roles of glutamate receptors and the mammalian target of rapamycin (mTOR) signaling pathway in activity-dependent dendritic protein synthesis in hippocampal neurons. J Biol Chem. 2006; 281:18802–18815. [PubMed: 16651266]

Gruenberg J, Stenmark H. The biogenesis of multivesicular endosomes. Nat Rev Mol Cell Biol. 2004; 5:317–323. [PubMed: 15071556]

Gulati P, Gaspers LD, Dann SG, Joaquin M, Nobukuni T, Natt F, Kozma SC, Thomas AP, Thomas G. Amino acids activate mTOR complex 1 via Ca2+/CaM signaling to hVps34. Cell Metab. 2008; 7:456–465. [PubMed: 18460336]

Hendry SH, Jones EG, Emson PC, Lawson DE, Heizmann CW, Streit P. Two classes of cortical GABA neurons defined by differential calcium binding protein immunoreactivities. Exp Brain Res. 1989; 76:467–472. [PubMed: 2767197]

Herman PK, Emr SD. Characterization of VPS34, a gene required for vacuolar protein sorting and vacuole segregation in Saccharomyces cerevisiae. Mol Cell Biol. 1990; 10:6742–6754. [PubMed: 2247081]

Johnson EE, Overmeyer JH, Gunning WT, Maltese WA. Gene silencing reveals a specific function of hVps34 phosphatidylinositol 3-kinase in late versus early endosomes. J Cell Sci. 2006; 119:1219–1232. [PubMed: 16522686]

Juhasz G, Hill JH, Yan Y, Sass M, Baehrecke EH, Backer JM, Neufeld TP. The class III PI(3)K Vps34 promotes autophagy and endocytosis but not TOR signaling in Drosophila. J Cell Biol. 2008; 181:655–666. [PubMed: 18474623]

Kelleher RJ 3rd, Govindarajan A, Tonegawa S. Translational regulatory mechanisms in persistent forms of synaptic plasticity. Neuron. 2004; 44:59–73. [PubMed: 15450160]

Lee JA, Beigneux A, Ahmad ST, Young SG, Gao FB. ESCRT-III dysfunction causes autophagosome accumulation and neurodegeneration. Curr Biol. 2007; 17:1561–1567. [PubMed: 17683935]

Lein ES, Hawrylycz MJ, Ao N, Ayres M, Bensinger A, Bernard A, Boe AF, Boguski MS, Brockway KS, Byrnes EJ, Chen L, Chen TM, Chin MC, Chong J, Crook BE, Czaplinska A, Dang CN, Datta S, Dee NR, Desaki AL, Desta T, Diep E, Dolbeare TA, Donelan MJ, Dong HW, Dougherty JG, Duncan BJ, Ebbert AJ, Eichele G, Estin LK, Faber C, Facer BA, Fields R, Fischer SR, Fliss TP, Frensley C, Gates SN, Glattfelder KJ, Halverson KR, Hart MR, Hohmann JG, Howell MP, Jeung DP, Johnson RA, Karr PT, Kawal R, Kidney JM, Knapik RH, Kuan CL, Lake JH, Laramee AR, Larsen KD, Lau C, Lemon TA, Liang AJ, Liu Y, Luong LT, Michaels J, Morgan JJ, Morgan RJ, Mortrud MT, Mosqueda NF, Ng LL, Ng R, Orta GJ, Overly CC, Pak TH, Parry SE, Pathak SD, Pearson OC, Puchalski RB, Riley ZL, Rockett HR, Rowland SA, Royall JJ, Ruiz MJ, Sarno NR, Schaffnit K, Shapovalova NV, Sivisay T, Slaughterbeck CR, Smith SC, Smith KA, Smith BI, Sodt AJ, Stewart NN, Stumpf KR, Sunkin SM, Sutram M, Tam A, Teemer CD, Thaller C, Thompson CL, Varnam LR, Visel A, Whitlock RM, Wohnoutka PE, Wolkey CK, Wong VY, Wood M, Yaylaoglu MB, Young RC, Youngstrom BL, Yuan XF, Zhang B, Zwingman TA, Jones AR. Genome-wide atlas of gene expression in the adult mouse brain. Nature. 2007; 445:168–176. [PubMed: 17151600]

Lencz T, Lambert C, DeRosse P, Burdick KE, Morgan TV, Kane JM, Kucherlapati R, Malhotra AK. Runs of homozygosity reveal highly penetrant recessive loci in schizophrenia. Proc Natl Acad Sci U S A. 2007; 104:19942–19947. [PubMed: 18077426]

Levine B, Klionsky DJ. Development by self-digestion: molecular mechanisms and biological functions of autophagy. Dev Cell. 2004; 6:463–477. [PubMed: 15068787]

Malinow R, Malenka RC. AMPA receptor trafficking and synaptic plasticity. Annu Rev Neurosci. 2002; 25:103–126. [PubMed: 12052905]

Nixon RA. Endosome function and dysfunction in Alzheimer's disease and other neurodegenerative diseases. Neurobiol Aging. 2005; 26:373–382. [PubMed: 15639316]

Nobukuni T, Kozma SC, Thomas G. hvps34, an ancient player, enters a growing game: mTOR Complex1/S6K1 signaling. Curr Opin Cell Biol. 2007; 19:135–141. [PubMed: 17321123]

Oh MC, Derkach VA. Dominant role of the GluR2 subunit in regulation of AMPA receptors by CaMKII. Nat Neurosci. 2005; 8:853–854. [PubMed: 15924137]

Parsons RG, Gafford GM, Helmstetter FJ. Translational control via the mammalian target of rapamycin pathway is critical for the formation and stability of long-term fear memory in amygdala neurons. J Neurosci. 2006; 26:12977–12983. [PubMed: 17167087]

Patki V, Lawe DC, Corvera S, Virbasius JV, Chawla A. A functional PtdIns(3)P-binding motif. Nature. 1998; 394:433–434. [PubMed: 9697765]

Pekny M, Nilsson M. Astrocyte activation and reactive gliosis. Glia. 2005; 50:427–434. [PubMed: 15846805]

Petiot A, Faure J, Stenmark H, Gruenberg J. PI3P signaling regulates receptor sorting but not transport in the endosomal pathway. J Cell Biol. 2003; 162:971–979. [PubMed: 12975344]

Petiot A, Ogier-Denis E, Blommaart EF, Meijer AJ, Codogno P. Distinct classes of phosphatidylinositol 3′-kinases are involved in signaling pathways that control macroautophagy in HT-29 cells. J Biol Chem. 2000; 275:992–998. [PubMed: 10625637]

Reddy PH, Williams M, Charles V, Garrett L, Pike-Buchanan L, Whetsell WO Jr, Miller G, Tagle DA. Behavioural abnormalities and selective neuronal loss in HD transgenic mice expressing mutated full-length HD cDNA. Nat Genet. 1998; 20:198–202. [PubMed: 9771716]

Skibinski G, Parkinson NJ, Brown JM, Chakrabarti L, Lloyd SL, Hummerich H, Nielsen JE, Hodges JR, Spillantini MG, Thusgaard T, Brandner S, Brun A, Rossor MN, Gade A, Johannsen P, Sorensen SA, Gydesen S, Fisher EM, Collinge J. Mutations in the endosomal ESCRTIII-complex subunit CHMP2B in frontotemporal dementia. Nat Genet. 2005; 37:806–808. [PubMed: 16041373]

Slipczuk L, Bekinschtein P, Katche C, Cammarota M, Izquierdo I, Medina JH. BDNF activates mTOR to regulate GluR1 expression required for memory formation. PLoS One. 2009; 4:e6007. [PubMed: 19547753]

Sofroniew MV. Molecular dissection of reactive astrogliosis and glial scar formation. Trends Neurosci. 2009; 32:638–647. [PubMed: 19782411]

Soreghan B, Thomas SN, Yang AJ. Aberrant sphingomyelin/ceramide metabolic-induced neuronal endosomal/lysosomal dysfunction: potential pathological consequences in age-related neurodegeneration. Adv Drug Deliv Rev. 2003; 55:1515–1524. [PubMed: 14597144]

Spinosa MR, Progida C, De Luca A, Colucci AM, Alifano P, Bucci C. Functional characterization of Rab7 mutant proteins associated with Charcot-Marie-Tooth type 2B disease. J Neurosci. 2008; 28:1640–1648. [PubMed: 18272684]

Stopkova P, Saito T, Papolos DF, Vevera J, Paclt I, Zukov I, Bersson YB, Margolis BA, Strous RD, Lachman HM. Identification of PIK3C3 promoter variant associated with bipolar disorder and schizophrenia. Biol Psychiatry. 2004; 55:981–988. [PubMed: 15121481]

Takegawa K, DeWald DB, Emr SD. Schizosaccharomyces pombe Vps34p, a phosphatidylinositol-specific PI 3-kinase essential for normal cell growth and vacuole morphology. J Cell Sci. 1995; 108 (Pt 12):3745–3756. [PubMed: 8719881]

Takei N, Inamura N, Kawamura M, Namba H, Hara K, Yonezawa K, Nawa H. Brain-derived neurotrophic factor induces mammalian target of rapamycin-dependent local activation of translation machinery and protein synthesis in neuronal dendrites. J Neurosci. 2004; 24:9760–9769. [PubMed: 15525761]

Tang R, Zhao X, Fang C, Tang W, Huang K, Wang L, Li H, Feng G, Zhu S, Liu H, He L, Shi Y. Investigation of variants in the promoter region of PIK3C3 in schizophrenia. Neurosci Lett. 2008; 437:42–44. [PubMed: 18420347]

Viviani B, Corsini E, Binaglia M, Galli CL, Marinovich M. Reactive oxygen species generated by glia are responsible for neuron death induced by human immunodeficiency virus-glycoprotein 120 in vitro. Neuroscience. 2001; 107:51–58. [PubMed: 11744246]

Wu C, Cui B, He L, Chen L, Mobley WC. The coming of age of axonal neurotrophin signaling endosomes. J Proteomics. 2009; 72:46–55. [PubMed: 19028611]

Wurmser AE, Gary JD, Emr SD. Phosphoinositide 3-kinases and their FYVE domain-containing effectors as regulators of vacuolar/lysosomal membrane trafficking pathways. J Biol Chem. 1999; 274:9129–9132. [PubMed: 10092582]

Xu B, Zang K, Ruff NL, Zhang YA, McConnell SK, Stryker MP, Reichardt LF. Cortical degeneration in the absence of neurotrophin signaling: dendritic retraction and neuronal loss after removal of the receptor TrkB. Neuron. 2000; 26:233–245. [PubMed: 10798407]

Zeng X, Overmeyer JH, Maltese WA. Functional specificity of the mammalian Beclin-Vps34 PI 3-kinase complex in macroautophagy versus endocytosis and lysosomal enzyme trafficking. J Cell Sci. 2006; 119:259–270. [PubMed: 16390869]

Zhou X, Wang L, Hasegawa H, Amin P, Han BX, Kaneko S, He Y, Wang F. Deletion of PIK3C3/Vps34 in sensory neurons causes rapid neurodegeneration by disrupting the endosomal but not the autophagic pathway. Proc Natl Acad Sci U S A. 2010; 107:9424–9429. [PubMed: 20439739]

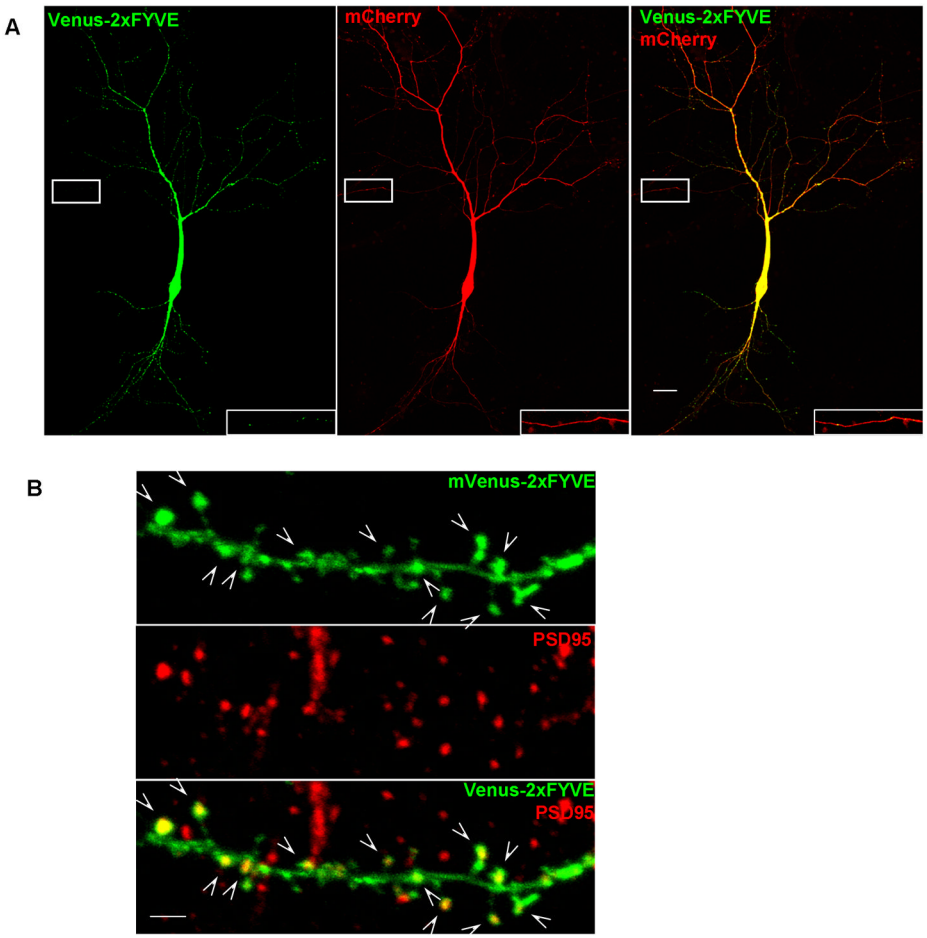

Figure 1. Distribution of PI3P in cultured neurons revealed by mVenus-2xFYVE fusion protein

A. Confocal images showing the intracellular distribution of PI3P in a 13 D.I.V. hippocampal neuron cotransfected with mVenus-2xFYVE (green) and mCherry (red). The image was taken using the tiling function and multiple images were stitched together by the software automatically. The image was significantly over-exposed in order to detect the localization of PI3P in high order branches. PI3P punctae labeled by mVenus-2xFYVE are detected in both dendrites and in axon. The insets are high-power magnification of the boxed axon regions. Scale bar: 20 μm.

B. Confocal images showing partial co-localization of PI3P, as revealed by mVenus-2xFYVE (green), with postsynaptic marker PSD95 (red) in cultures neurons. Arrows indicate the co-localization. Scale bar:2μm.

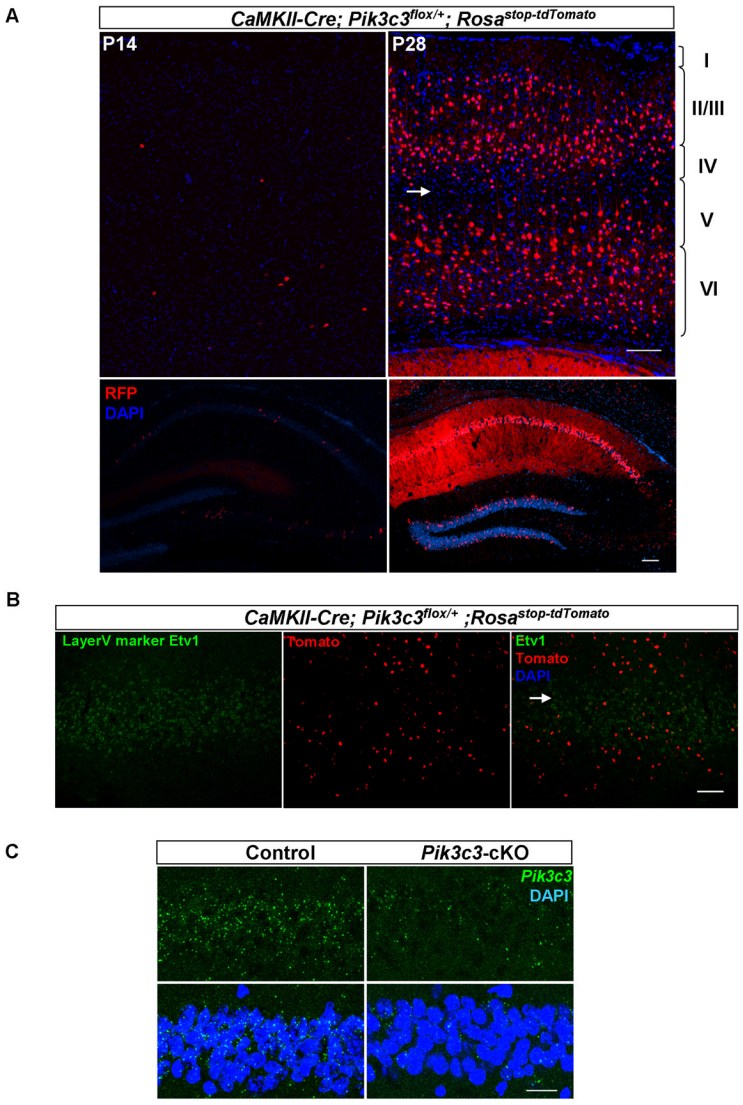

Figure 2. Patterns of *CaMKII*-Cre mediated deletion of *Pik3c3* in the brain

A. Representative coronal sections of cortex (upper panel) and hippocampus (lower panel) from P14 (left) and P28 (right) *CaMKII* Cre; *Pik3c3*$^{flox/+}$; *Rosa*$^{STOP\text{-}tdTomato}$ mice showing the expression of *tomato* gene revealed by anti-RFP immunostaining. The image was taken using the tiling function and multiple images were stitched together automatically. At P14, a small amount of neurons express tomato in the cortex as well CA1, CA3 and DG regions at P14 (left panel). After P28, more than 95% of CA1 hippocampal neurons and about 22.8% of cortical neurons express tomato. Arrow indicates layer V where very few cells are tomato-positive. Scale bar: 100 μm.

B. Representative images of fluorescence in situ hybridization with probes for layer V marker Etv1 (green) and tomato (red) on sagittal sections of P28 *CaMKII*-Cre; *Pik3c3*$^{flox/+}$; *Rosa*$^{stop\text{-}tdTomato}$ mice.

C. Fluorescence in situ hybridization using a *Pik3c3* (green) probe verifies the largely diminished expression of *Pik3c3* in CA1 hippocampal neurons in *Pik3c3*-cKO mutant as compared with those in control heterozygous at P28. Scale bar: 20 μm.

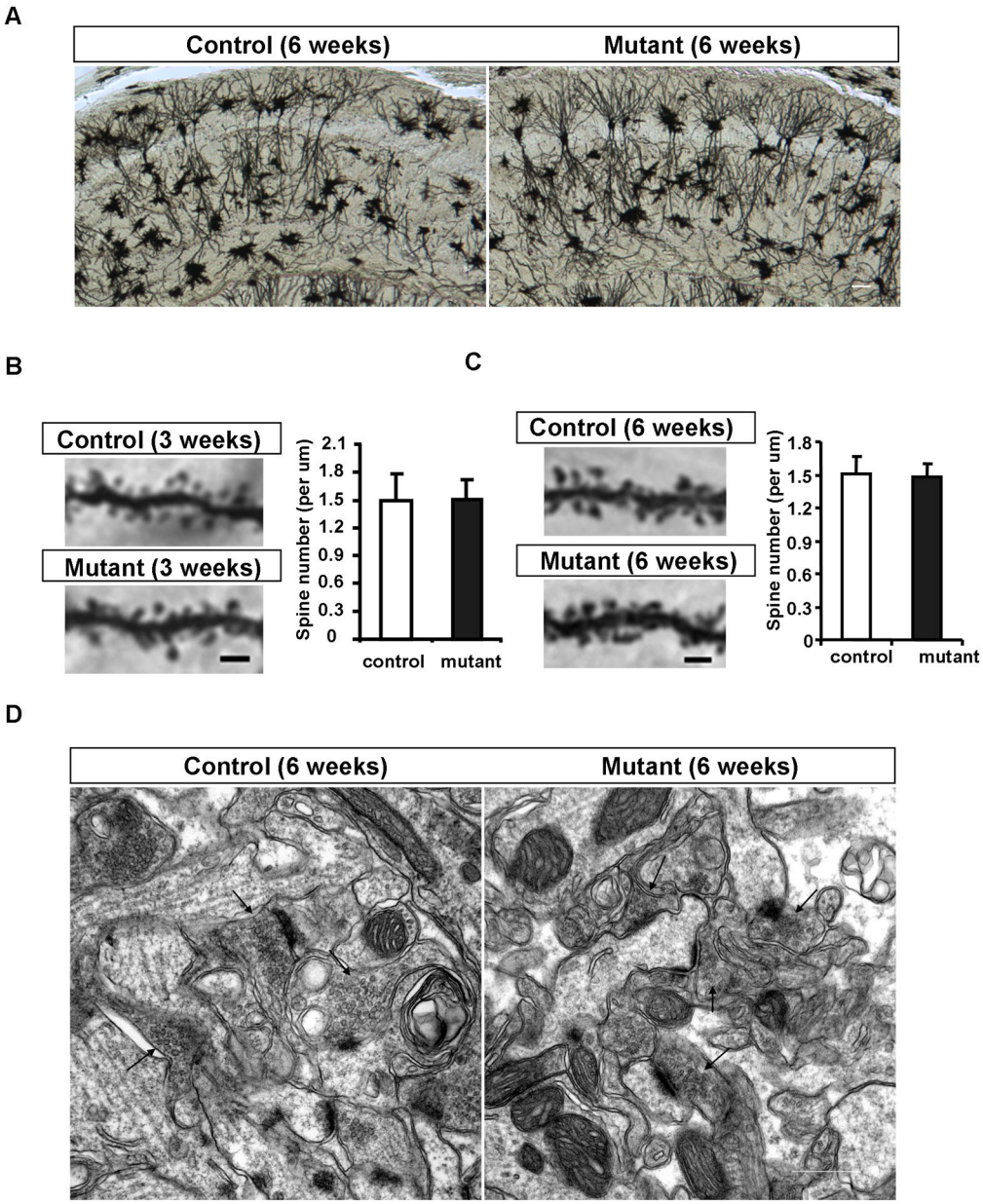

Figure 3. Normal neuronal morphology and synapse ultrastructure of *Pik3c3*-cKO at the age of 6-week

A. Representative image of Golgi staining of hippocampal neurons in the CA1 region from 6-week old controls and *Pik3c3*-cKO mutant mice. Scale bar: 100 μm

B. Representative images of the first order branch of apical dendrites within lucidum-radiatum region from control and *Pik3c3*-cKO mutant CA1 hippocampal neurons at the age of 3 weeks. Scale bar: 2 μm. Histogram shows the spine density (averaged from 24 randomly selected sections from different mice for each genotype). p>0.9, Two-tailed paired t test.

C. Representative images of the first order branch of apical dendrites within lucidum-radiatum region from control and *Pik3c3*-cKO mutant CA1 hippocampal neurons at the age of 6 weeks. Scale bar: 2 μm. Histogram shows the spine density (averaged from 24 randomly selected sections from different mice for each genotype). p>0.9, Two-tailed paired

t test. D. Representative electron microphotographs of the CA1 region from control and *Pik3c3*-cKO mice at age of 6 weeks. Scale bar, 0.5 μm.

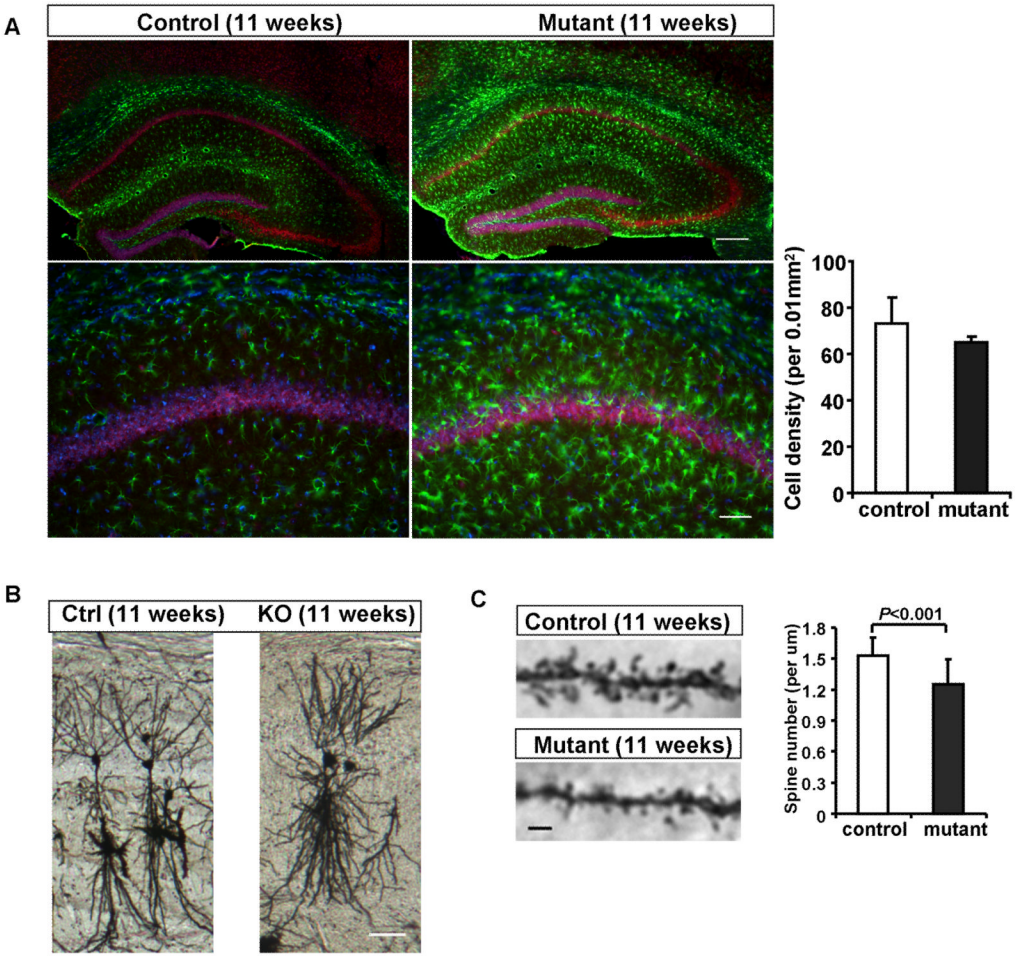

Figure 4. Gliosis and reduction of dendritic spines precede neuronal loss in the *Pik3c3*-cKO hippocampus at the age of 11-week

A. Upper panel: Immunostaining with anti-NeuN (red) and anti-GFAP (green) shows increased GFAP fluorescence intensity and positive cells in the mutant hippocampal formation compared with control in 11-week old mice (Scale bar: 100 μm). Lower panel: high-power magnification of the CA1 region (Scale bar: 50 μm). Right: Quantification of CA1 hippocampal neuron density at age of 11 weeks. Histograms show the density of NeuN positive cells (average ± SEM), N=12~16 randomly selected sections from different mice for each genotype. $p>0.4$, Two-tailed paired t test.

B. Representative images of Golgi staining of hippocampal neurons in the CA1 region from 11 weeks old control and *Pik3c3*-cKO mutant mice. Scale bar: 100 μm.

C. Representative images of the first order branch of apical dendrites within lucidum-radiatum region from the control and *Pik3c3*-cKO mutant CA1 hippocampal neuron at age of 11 weeks. Scale bar: 2 μm. Histogram shows the spine density (N=26 randomly selected sections from different mice for each genotype). $p<0.01$, Two-tailed paired t test.

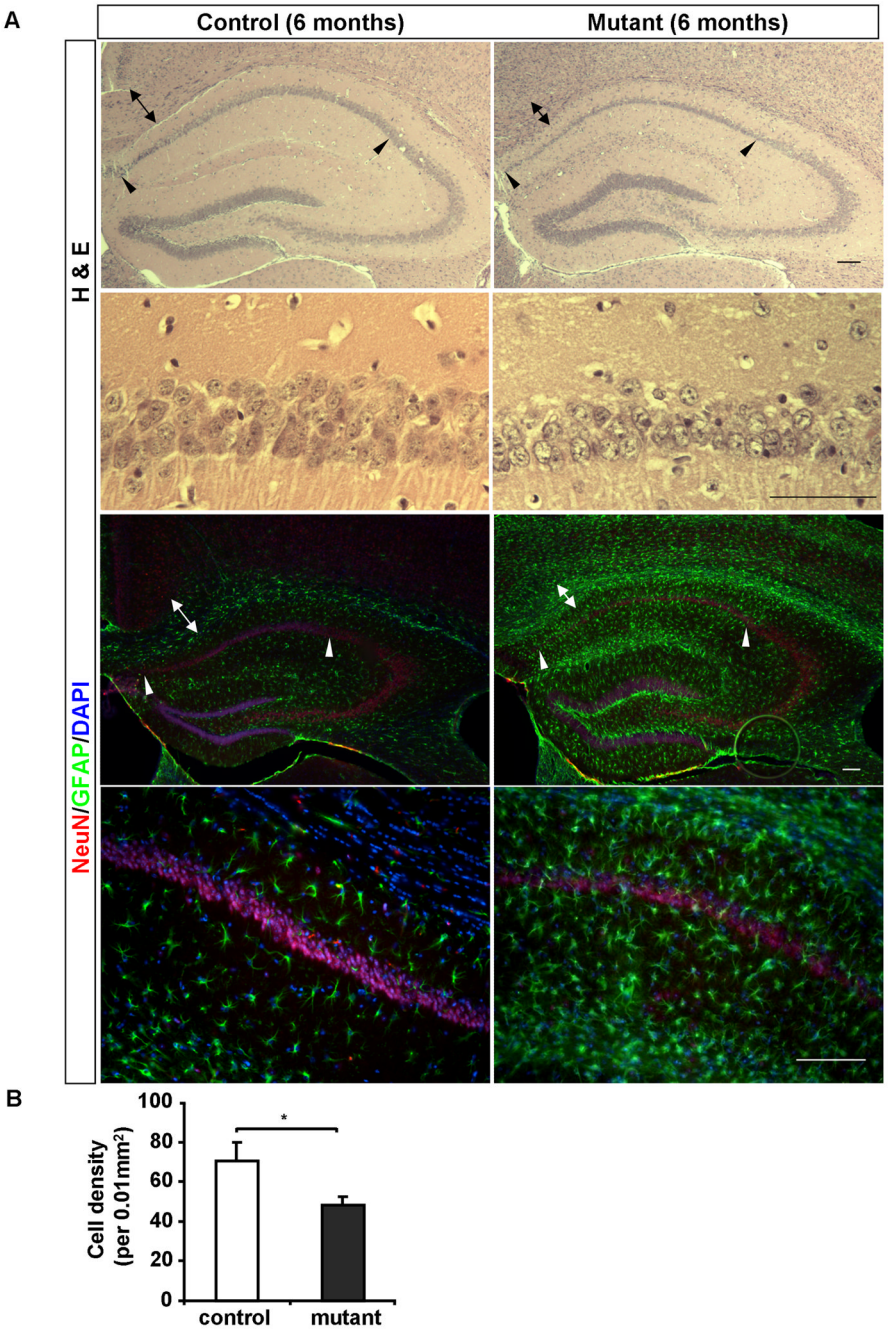

Figure 5. Profound neuronal loss and gliosis in the *Pik3c3*-cKO hippocampus at 6-month of age

A. Upper panel: Representative H& E staining of the hippocampal formation from 6-month old mice shows compressed CA1 pyramidal layer in the *Pik3c3-cKO* mutant mice. Lower panel: higher magnifications of the stained CA1 region. Arrowheads indicate the CA1 region. Arrows indicate the axon track of the external capsule. Scale bar: 100 μm.

B. Upper panel: Immunostaining of the hippocampal formation using anti-NeuN (red) and anti-GFAP (green) reveals gliosis and thinning of CA1 region in the *Pik3c3-cKO* mutant mice. Lower panel: higher magnification of the immunostained CA1 region. Arrowheads indicate the CA1 region. Arrows indicate the axon track of the external capsule. Scale bar: 100 μm.

C. Quantifications of CA1 hippocampal neuron density at the age of 6 months. Histograms show the average density of NeuN positive cells (average ± SEM). N=12–16 randomly selected sections from different mice for each genotype. Two-tailed paired t test; * $p<0.05$

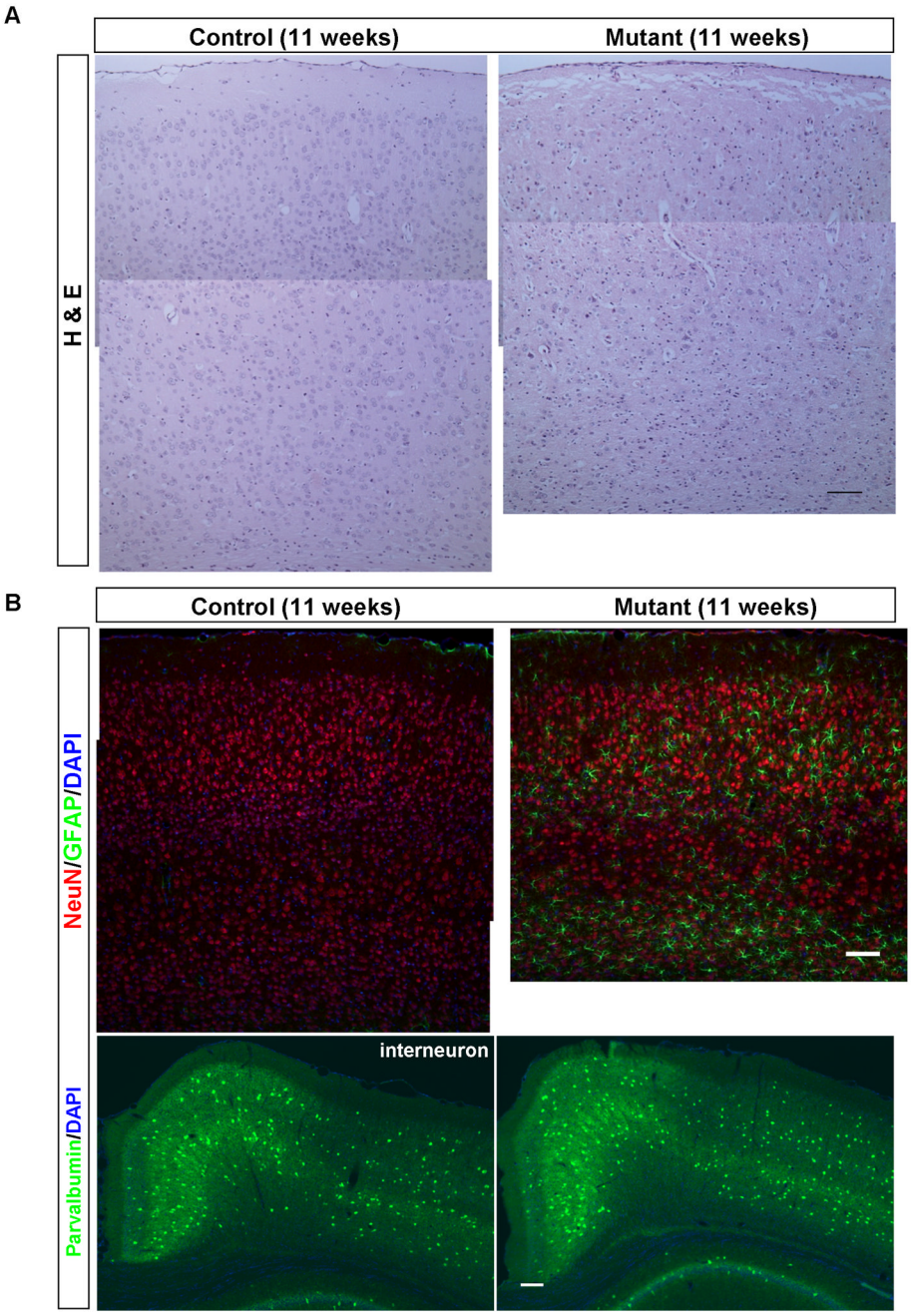

Figure 6. Gliosis and excitatory neuronal loss occur in the 11-week old *Pik3c3*-cKO cortex

A. Representative H&E staining of cortex from control and *Pik3c3*-cKO mutant mice shows reduced thickness of cortex and increased amount of darkly-stained nuclei in the mutant mice.

B. Upper panel: Immunostaining of the cortex using anti-NeuN (red) and anti-GFAP (green) shows apparent neuronal loss and a dramatic increase in GFAP fluorescence intensity as well GFAP-positive cell number in *Pik3c3*-cKO mutant mice. Lower panel: immunostaining of the cortex using anti-parvalbumin (green, interneuron marker). Scale bar: 100 μm.

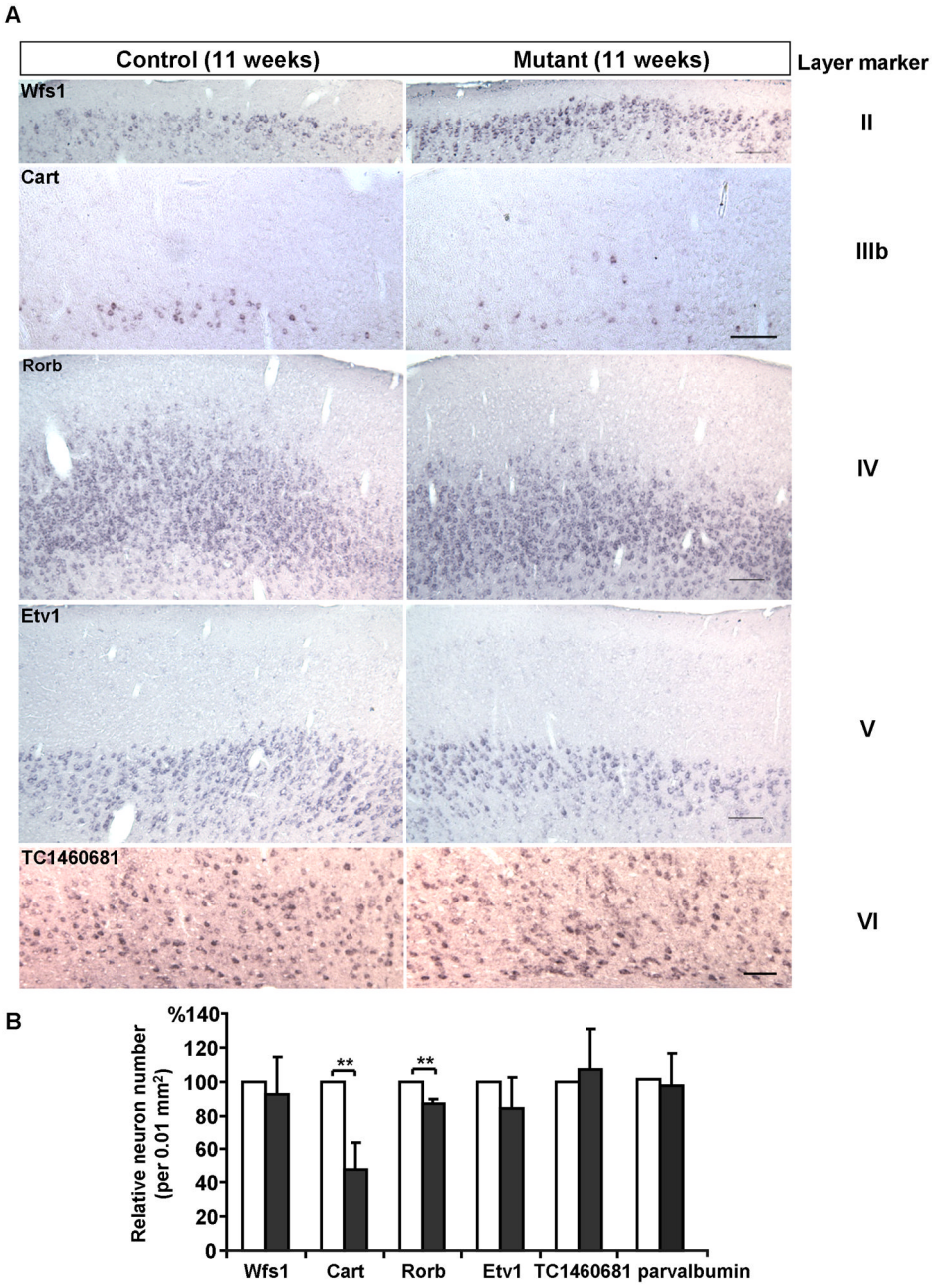

Figure 7. Loss of layer III and IV marker expressing cortical neurons in the 11-week old *Pik3c3*-cKO cortex

A. Representative images of in situ hybridization with Wolfram syndrome 1 homolog (Wfs1, layer II marker), cocaine and amphetamine regulated transcript (Cart, layer IIIb marker), RAR-related orphan receptor beta (Rorb, layer IV marker), ets variant gene 1 (Etv1, layer V marker) and TC1460681 (layer VI marker) on coronal sections of 11 weeks old control and *Pik3c3*-cKO mutant cortex. Scale bar: 100 μm.

B. Relative area density of layer marker expressing cells in 11 weeks old control and *Pik3c3*-cKO mutant mice. Graphs show the average percent of positive cells (average ± s.d). N=16~20 randomly selected sections from different mice for each genotype. Two-tailed paired t test; double asterisk, $p<0.01$.

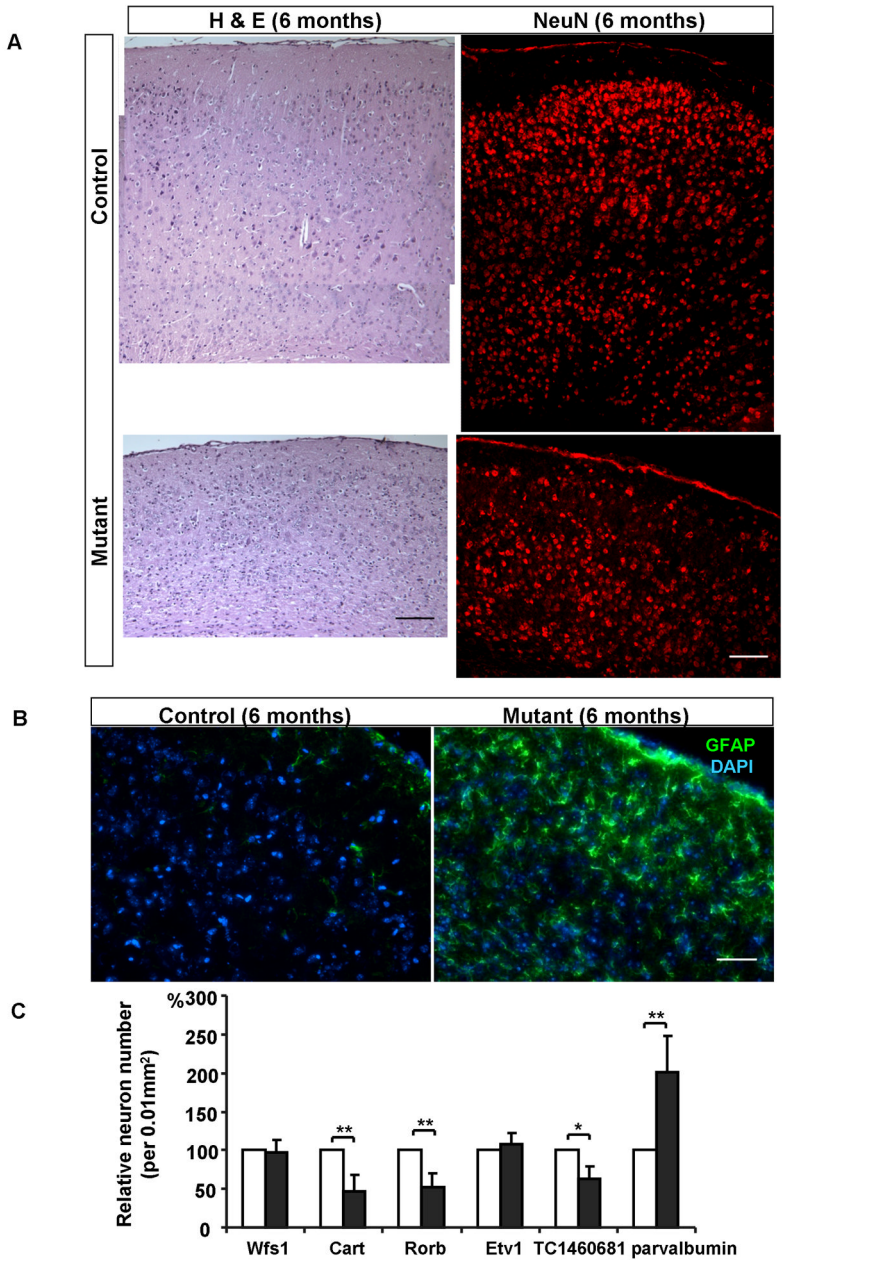

Figure 8. Extensive neuronal loss and gliosis in the *Pik3c3*-cKO cortex at 6 months

A. Left panel: H & E staining of cortex from control and *Pik3c3*-cKO mutant show significant shrinkage of the cortex and increased amount of pyknotic nuclei in the mutant mice at age of 6 months. Right panel: immunostaining of the cortex using anti-NeuN (red) shows a dramatic neuronal loss in *Pik3c3*-cKO mutant mice as compared to that in the control. Scale bar: 100 μm.

B. Immunostaining of the cortex using anti-GFAP (green) reveals a significantly increase in both the fluorescence intensity and positive cell numbers in 6 months old *Pik3c3*-cKO mutant mice. Scale bar: 50 μm.

C. Relative area density of Wfs1, Cart, Rorb, Etv1, TC1460681 and parvalbumin expressing cells in 6 months old control and *Pik3c3*-cKO mutant mice. Graphs show the relative

percentage of positive cells (average ± s.d). N=16~20 randomly selected sections from different mice for each genotype. Two-tailed paired t test; **, $p<0.01$.

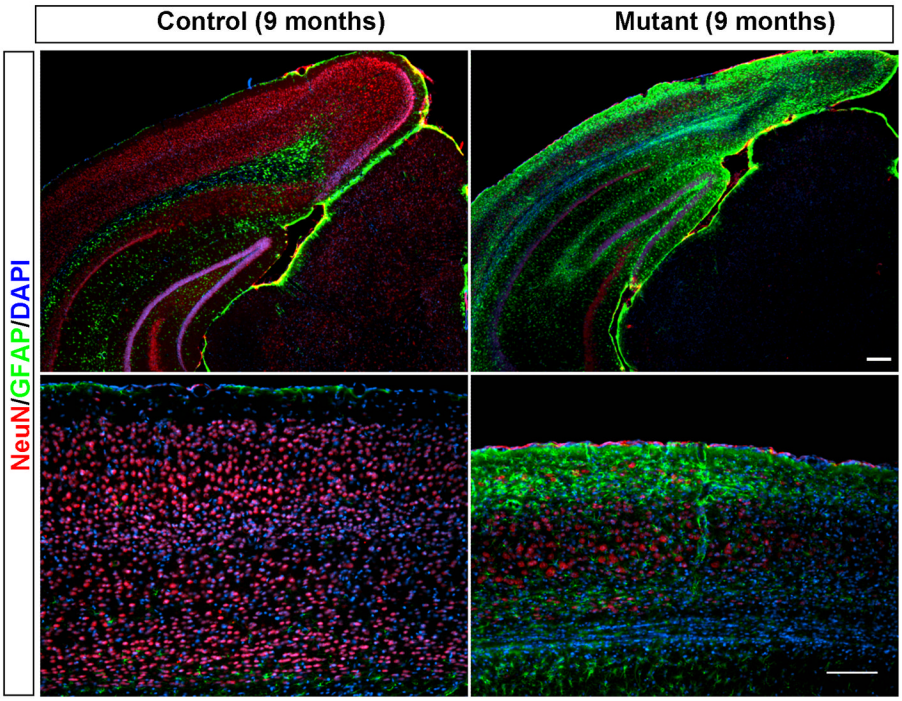

Figure 9. Massive neuronal loss and gliosis in the *Pik3c3*-cKO mutant at 9-month old age

Immunostaining of the cortex of 9 month old mice using anti-NeuN (red) and anti-GFAP (green) shows massive neuronal loss and gliosis in the *pik3c3*-cKO mutant. Lower panel: higher magnification of the stained cortex. Scale bar: 100 μm.

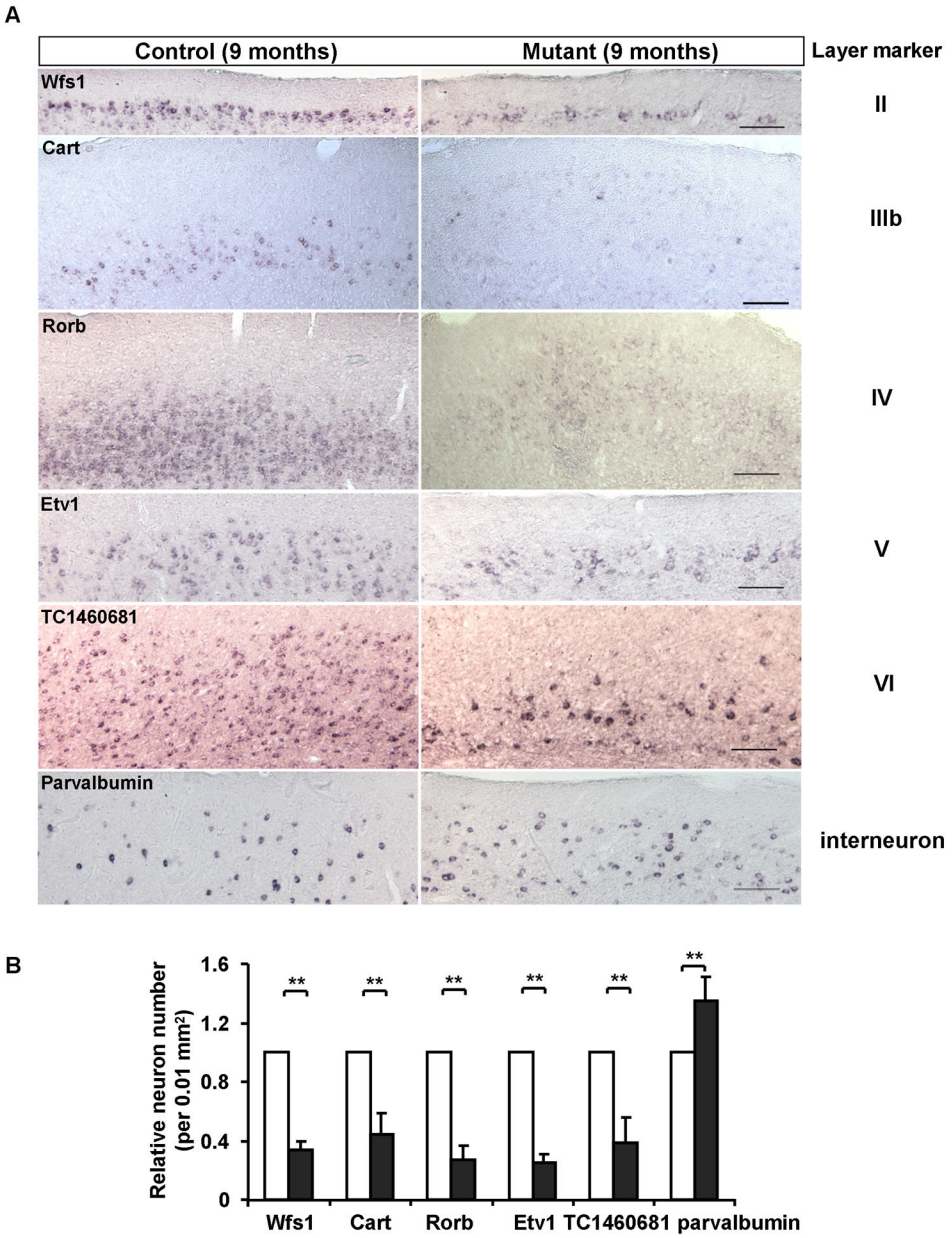

Figure 10. Extensive loss of all types of neurons in the cortex of the *Pik3c3*-cKO mutant at the age of 9 months

A. Representative images of in situ hybridization with Wfs1, Cart, Rorb, Etv1, TC1460681 and parvalbumin on coronal sections of 9 months old control and *Pik3c3*-cKO mutant cortex. Scale bar: 100 μm.

B. Relative number of layer marker expressing cells in 9 months old control and *Pik3c3*-cKO mutant mice. Graphs show the relative percentage of marker-positive cells (average ± s.d). N=16~20 randomly selected sections from different mice for each genotype. Two-tailed paired t test; **, $p<0.01$.

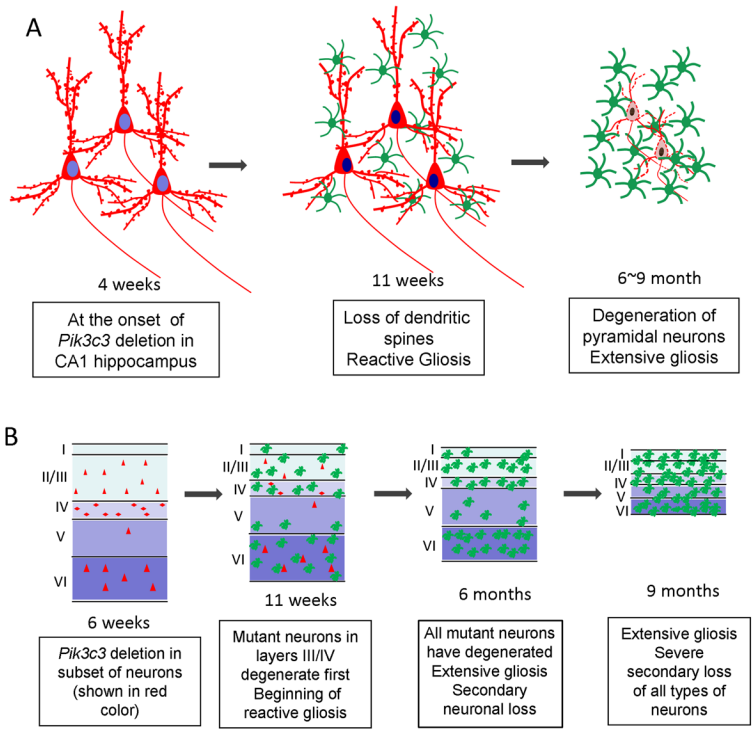

Figure 11. Schematic models of pathologic changes in the mutant brain over times

A. Schematic drawing depicts the temporal phenotype of the CA1 hippocampal neuron in the mutant brain. Hippocampal neurons in the CA1 region appear normal at 4 weeks when *Pik3c3* deletion occurs. Seven weeks later, hippocampal neurons show loss of dendritic spines accompanied with apparent gliosis. At late stage, extensive pyramidal neuronal degeneration and gliosis occur.

B. Schematic model summarizes phenotypes observed in the mutant cortex. A small subset of cortical neurons undergo CamKII-Cre mediated *Pik3c3* deletion, and the cortex appears normal at 4~6 weeks. Layer III and IV mutant cortical neurons degenerate which is associated with reactive gliosis at 11 weeks. At 6 months, all *Pik3c3* deficient cortical neurons degenerate, some loss of wildtype neurons begins and extensive gliosis occurs. At late stage, severe loss of all types neurons occurs, concurrent with extensive gliosis that covers the remaining cortex.